STRESS-STRAIN RELATIONS FOR DRY AND SATURATED SANDS PART II: PREDICTIONS

ANDRZEJ SAWICKI
WALDEMAR ŚWIDZIŃSKI

Institute of Hydro-Engineering, IBW PAN, Gdańsk-Oliwa, Poland

e-mail: as@ibwpan.gda.pl; waldek@ibwpan.gda.pl

In the second part of the paper, the incremental constitutive model, described in details in Part I, was verified against the experimental data obtained from the stress paths different that those used for model calibration. The differential equations defining the model were integrated for various stress paths such as anisotropic consolidation including oedometric conditions, standard triaxial compression, spherical unloading of fully drained soil as well and shearing of water saturated sand in undrained conditions. The behaviour of both initially contractive and dilative soil was considered. Theoretical predictions were compared with the respective experimental data. In all cases examined, the agreement between predictions and experimental data seems to be quite good.

Key words: granular soils, stress-strain characteristics, pre-failure behaviour, instability, liquefaction, anisotropy

1. Introduction

In the second part of this paper, some applications of the incremental constitutive model presented in Part I are shown in order to predict the pre-failure behaviour of sand for loading paths different from those used for calibration. Recall that the model has been calibrated for the strains that develop for the stress paths OA and ABC, in the case of loading, and AO and CBA in the case of unloading. The behaviour predicted for the other loading paths, compared with the experimental data, serves as a kind of validation of the model proposed. The predictions shown in this part of the present paper are based on integration of Eqs. (4.1) in Part I, along those other loading paths.

2. Anisotropic consolidation

The anisotropic consolidation takes place along the stress path OD, see Fig. 1 in Part I. Note that along this path, both p' and q change, but the ratio $\eta = q/p'$ remains constant. In the case considered, there is

$$\eta = \frac{3(1-K)}{1+2K} \tag{2.1}$$

where $K = \sigma_3/\sigma_1 = \text{const}$.

Consider two different cases of anisotropic consolidation, namely $\eta < \eta'$ and $\eta > \eta'$, where η' corresponds to the instability line. Recall that the region in the stress space below the instability line is considered as a region of stable behaviour, whilst the region above this line corresponds to unstable behaviour of the soil. Figure 1 shows the experimental results, representing the development of volumetric and deviatoric strains in the soil, for the previously mentioned cases, see Świdziński (2006). These strains were developed along the stress paths $\eta = 0.375$ ($K = 0.7$) and $\eta = 1.179$ ($K = 0.34$). The results presented in Fig. 1 can be approximated by the following formulae

$$\begin{array}{llll} \varepsilon_v = 7.1\sqrt{p'} & \varepsilon_q \approx 0 & \text{for} & \eta = 0.375 \\ \varepsilon_v = 2.52\sqrt{p'} & \varepsilon_q = 13.61\sqrt{p'} & \text{for} & \eta = 1.179 \end{array} \tag{2.2}$$
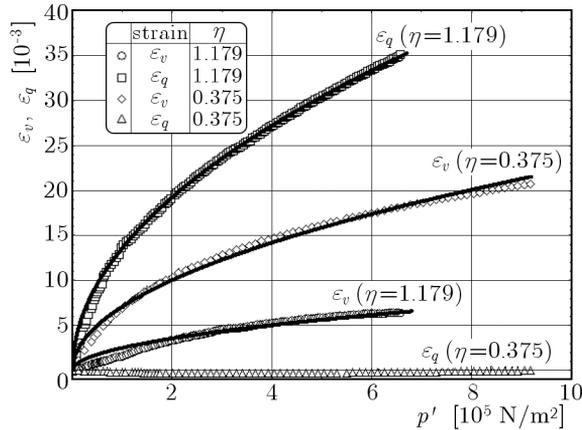

Fig. 1. Strains developed along two paths of anisotropic consolidation

2.1. The case $\eta = 0.375$

This case corresponds to the region below the instability line, and the respective incremental equations take the following form

$$d\varepsilon_v = \Big(\frac{A_v}{2} + 4c_1\eta^4\Big)\frac{1}{\sqrt{p'}}dp' = C_v\frac{1}{\sqrt{p'}}dp'$$
$$d\varepsilon_q = \Big(\frac{A_q}{2} + \eta b_1 b_2 \exp(b_2\eta)\Big)\frac{1}{\sqrt{p'}}dp' = C_q\frac{1}{\sqrt{p'}}dp' \tag{2.3}$$

Note that in the case considered, one of the independent stress variables was replaced by the other, i.e. $dq = \eta dp'$. Integration of the above equations with zero initial conditions leads to the following expressions

$$\varepsilon_v = 2C_v\sqrt{p'} \qquad \varepsilon_q = 2C_q\sqrt{p'} \tag{2.4}$$

which are of the same shape as the analytical approximations of experimental data (2.2), so the qualitative agreement between the empirical results and theoretical predictions is good. Substitution of average material parameters, already presented in Part I of this paper leads to quantitative results. For the average coefficients: $A_v = 6.01$; $A_q = -0.95$; $c_1 = 2.97$; $b_1 = 0.023$; $b_2 = 6.245$ (remember about respective stress and strain units!) one obtains: $\varepsilon_v = 6.48\sqrt{p'}$ and $\varepsilon_q = 0.17\sqrt{p'}$, which differ a little from those obtained from the experiments, cf. Eq. (2.2). However, if we slightly change just two of these parameters, namely substitute $A_v = 6.5$ and $b_2 = 6$, we obtain respectively: $\varepsilon_v = 6.97\sqrt{p'}$ and $\varepsilon_q = 0.032\sqrt{p'}$ which are indeed very close to the experimental values.

2.2. The case $\eta = 1.179$

The stress path corresponding to this case is located in the region of potential instability, so assume that the incremental equations for the dilative soil are valid. The strains are given by Eqs. (2.4), but with different coefficients, namely

$$C_v = \frac{A_v}{2} + 2a_1\eta^2 + a_2\eta \qquad C_q = \frac{A_q}{2} + \eta b_1 b_2 \exp(b_2\eta) \tag{2.5}$$

Substitution of the following parameters: $A_v = 3.47$; $A_q = -0.53$; $a_1 = -1.0$; $a_2 = 2.0$; $b_1 = 0.00035$; $b_2 = 6.648$ leads to the following relations: $\varepsilon_v = 2.63\sqrt{p'}$ and $\varepsilon_q = 13.38\sqrt{p'}$, which are very close to empirical relations (2.2).

2.3. Strain paths

The experimental results and theoretical predictions previously presented can also be interpreted in terms of the principal strains, given by the following relation obtained from Eqs. (2.1)$_{3,4}$ in Part I

$$\varepsilon_1 = \frac{1}{3}\varepsilon_v + \varepsilon_q \qquad\qquad \varepsilon_3 = \frac{1}{3}\varepsilon_v - \frac{1}{2}\varepsilon_q \qquad\qquad (2.6)$$

For analytical approximations of experimental data (2.2), one obtains the following values of the ratio of principal strains $\varepsilon_1/\varepsilon_3 = 1$ for $\eta = 0.375$ and $\varepsilon_1/\varepsilon_3 = -2.42$ for $\eta = 1.179$. Respective predictions presented in Sections 2.1 and 2.2 give $\varepsilon_1/\varepsilon_3 = 1.12$ for $\eta = 0.375$ and $\varepsilon_1/\varepsilon_3 = -2.45$ for $\eta = 1.179$. In this case, the agreement is remarkable, cf. Fig. 2.
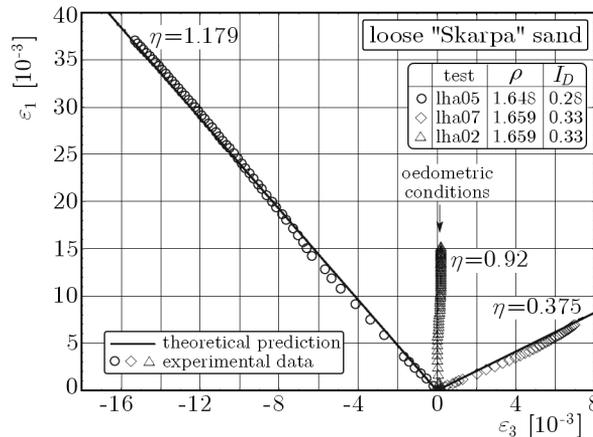

Fig. 2. Experimentally determined principal strain paths during anisotropic consolidation against theoretical predictions

3. Oedometric behaviour

3.1. Oedometric conditions

In the oedometric conditions, the lateral strains are equal to zero, which means that in the triaxial compression tests there should be $\varepsilon_3 = 0$, cf. one of the strain paths shown in Fig. 2 (after Świdziński, 2006). This path was obtained for the anisotropic consolidation defined by $\eta = 0.92$ ($K = 0.43$).

It should be noted that such experiments are difficult to perform in the triaxial apparatus as the lateral strain should be controlled. Such conditions are automatically realised in a standard oedometer, where the rigid wall imposes constrains on the horizontal deformations.

As the subsequent prediction of the incremental model proposed, the stress path corresponding to oedometric conditions will be determined, and the results of calculations will be compared with the experimental data. The value of η, corresponding to oedometric conditions, will be calculated from Eq. $(2.6)_2$, assuming $\varepsilon_3 = 0$, which in this case reduces to

$$\frac{\varepsilon_v}{\varepsilon_q} = \frac{3}{2} \qquad \text{or} \qquad \frac{d\varepsilon_v}{d\varepsilon_q} = \frac{3}{2} \qquad (3.1)$$

3.2. Initially loose soil

In the case of initially loose soil, Eq. (3.1) leads to the following relation for η

$$\frac{A_v}{2} + 4c_1\eta^4 - \frac{3}{4}A_q - \frac{3}{2}\eta b_1 b_2 \exp(b_2\eta) = 0 \qquad (3.2)$$

Substitution of the following parameters: $A_v = 6$; $A_q = -0.95$; $c_1 = 2.97$; $b_1 = 0.000335$; $b_2 = 8.32$ leads to the following equation

$$887.99 + 2841.56\eta^4 - \eta\exp(8.32\eta) = 0$$

The solution has been found numerically: $\eta = 0.985$ which corresponds to $K = 0.405$. Recall that the respective experimental values are $\eta = 0.92$ and $K = 0.43$, see Fig. 2. Note that the difference between theoretical predictions and experimental results is less than 6% in this case.

3.3. Initially dense soil

A similar technique has been applied to predict the oedometric behaviour of initially dense soil. Equation (3.1) takes the following form in this case

$$\frac{A_v}{2} + 2a_1\eta^2 + a_2\eta - \frac{3}{4}A_q - \frac{3}{2}\eta b_1 b_2 \exp(b_2\eta) = 0 \qquad (3.3)$$

Substitution of the following parameters: $A_v = 3.47$; $A_q = -0.53$; $a_1 = -1$; $a_2 = 2$; $b_1 = 0.00035$; $b_2 = 6.648$ leads to the following equation

$$611 - 573.03\eta^2 + 573.03\eta - \eta\exp(6.648\eta) = 0$$

with the solution $\eta = 0.973$ corresponding to $K = 0.41$. Recall that the experimental value of $K = 0.43$, see Fig. 2. Such a remarkable agreement can obviously be accidental. Note that, on one hand, we substitute into the respective equations the average values of sand parameters, determined experimentally. On the other hand, the prediction is compared with the independent result of just a single experiment. Anyway, in spite of such doubts, the agreement between predictions and empirical results seems to be quite good.

3.4.   Oedometric stress-strain curve

In classical oedometric investigations, the vertical stress-vertical strain curve is determined, i.e. $\varepsilon_1 = \varepsilon_1(\sigma_1')$. Such a curve can also be obtained from Eqs. (2.3). Note that in the case considered

$$d\varepsilon_v = d\varepsilon_1 \qquad d\varepsilon_q = \frac{2}{3}d\varepsilon_1 \qquad\qquad (3.4)$$

as ε_3 and $d\varepsilon_3$ are zero. There is also $\sigma_3' = K\sigma_1'$.

First, Eqs. (2.3) should be solved in order to determine the value of η, as shown in Sections 3.2 and 3.3. Then, the respective stress-strain curve can be determined either from Eq. $(2.3)_1$ or $(2.3)_2$. Integration of these equations leads to relations (2.4), which together with Eq. (3.4), gives the same results. For example, it follows from Eqs. $(2.4)_1$ and (3.4) that

$$\varepsilon_1 = 2C_v\sqrt{\frac{1+2K}{3}}\sqrt{\sigma_1'} = 2D\sqrt{\sigma_1'} \qquad\qquad (3.5)$$

where C_v is defined in Eq. $(2.3)_1$.

Substitution of the data from Section 3.2 gives: $\varepsilon_1 = 28.37\sqrt{\sigma_1'}$. The same result is obtained from Eqs. $(2.3)_2$, $(2.4)_2$ and (3.4), which can be easily checked by substitution. The investigations performed on other sands give the following values of the coefficient appearing in Eq. (3.5): $2D = 30$ for "Sobieszewo" sand or $2D = 25$ for "Lubiatowo" sand, see Sawicki and Świdziński (1998).

For the data from Section 2.2, one obtains $\varepsilon_1 = 2.73\sqrt{\sigma_1'}$. Figure 3 shows the oedometric stress-strain curve for "Skarpa" sand of the initial relative density $I_D = 0.86$. This curve can be approximated by the following formula: $\varepsilon_1 = 3.27\sqrt{\sigma_1'}$ which is indeed very close to the analytical prediction.
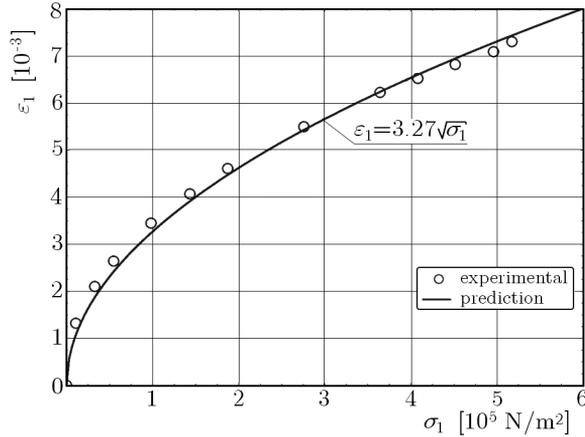
Fig. 3. Experimental oedometric stress-strain curve for "Skarpa" sand against the theoretical prediction

4.   Standard triaxial compression test

The standard compression test is much easier to perform in a conventional triaxial apparatus than the pure shearing at a constant mean stress, because it is not necessary in it to change the cell pressure. In such a standard test, the cell pressure is kept constant $(\sigma_3 = \text{const})$ and only the vertical stress σ_1 increases, which corresponds to the stress path AE in Fig. 1 in Part I, as both p and q increase according to Eqs. $(2.1)_{1,2}$ in Part I. In this special case, the stress increments are the following

$$dp' = \frac{1}{3}d\sigma_1' \qquad dq = d\sigma_1' = 3dp' \qquad (4.1)$$

Consider the case of initially contractive soil. The incremental equations are the following

$$d\varepsilon_v = \left(\frac{A_v}{2} + 12c_1\eta^3\right)\frac{1}{\sqrt{p'}}dp' \qquad d\varepsilon_q = \left(\frac{A_q}{2} + 3b_1b_2\exp(b_2\eta)\right)\frac{1}{\sqrt{p'}}dp' \qquad (4.2)$$

where relation (4.1) was taken into account.

There are two variables, namely p' and η, which are inter-related. In order to eliminate η from Eqs. (4.2), let us consider Fig. 4 from which it follows

$$\eta = 3\left(1 - \frac{p_A'}{p'}\right) \qquad (4.3)$$

where p_A' denotes the initial mean effective stress prior to the test.
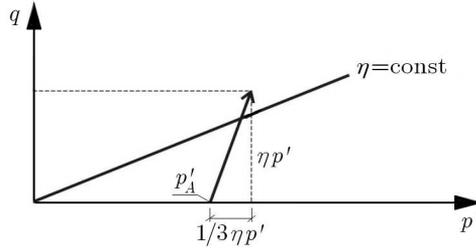
Fig. 4. Stress paths in standard triaxial tests. Geometrical relation between p' and η

Substitution of Eq. (4.3) into Eqs. (4.2) leads to the following relations which describe the development of pre-failure strains corresponding to the stress path AE from Fig. 1 in Part I

$$d\varepsilon_v = \left[\frac{A_v}{2} + 324c_1\left(1 - \frac{p'_A}{p'}\right)^3\right]\frac{1}{\sqrt{p'}}dp'$$

$$d\varepsilon_q = \left\{\frac{A_q}{2} + 3b_1b_2\exp\left[3b_2\left(1 - \frac{p'_A}{p'}\right)\right]\right\}\frac{1}{\sqrt{p'}}dp'$$

(4.4)

The above equations have been integrated numerically for the average values of material parameters (see Section 3.2 of Part I of this paper), which correspond to the initially contractive soil state and for the following initial conditions: $\varepsilon_v(p' = p'_A) = 0$ and $\varepsilon_q(p' = p'_A) = 0$. Figure 5 shows the results of computation against the experimental data. It can be seen that again qualitative and quantitative reproduction of the experimental results by the model proposed for the standard triaxial compression test carried out on the contractive soil is very good.

5. Unstable behaviour during spherical unloading

5.1. Experimental observations

A very interesting behaviour of initially loose sand is shown in Fig. 6, after Świdziński (2006). First, the soil samples were subjected to isotropic consolidation up to $p' = p'_A = 2 \cdot 10^5 \, \text{N/m}^2$. Then, each of three samples investigated was subjected to pure shearing, up to different deviatoric stress levels. Subsequently, the deviatoric stress was kept constant, and the mean stress p' reduced (spherical unloading). During the first part of this process (path BC in Fig. 6) the dilation takes place, i.e. the volume of soil increases. After reaching the
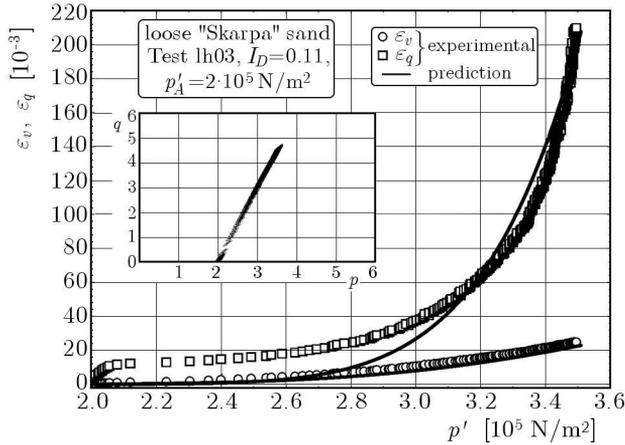
Fig. 5. Experimental and predicted stress-strain curves for standard tri-axial compression
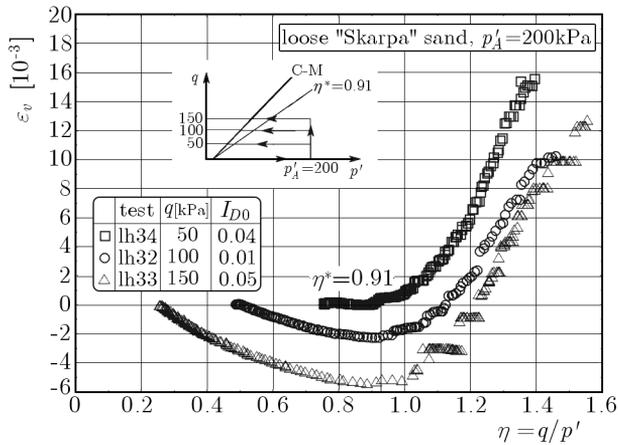
Fig. 6. Volumetric deformations of initially loose "Skarpa" sand during spherical unloading

instability line (point C in Fig. 6), the volumetric strains rapidly decrease, i.e. a sudden compaction takes place. This phenomenon is better visible in Fig. 7, where the data from Fig. 6 are shown in a different system of co-ordinates.

Similar experiments were carried out by Skopek *et al.* (1994). The authors designated the process of sudden decrease in volume as structural collapse of sand due to progressive destruction of the soil structure caused by isotropic unloading.
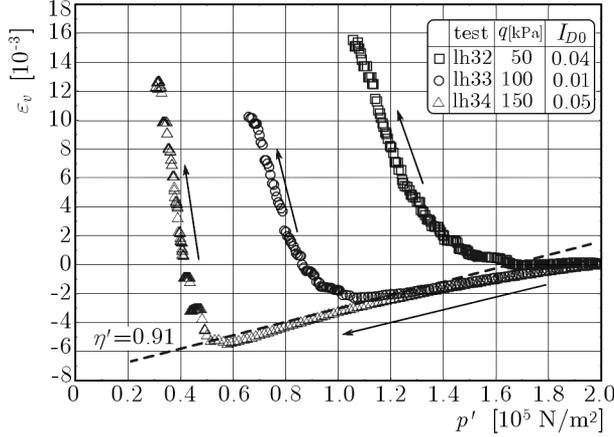
Fig. 7. Sudden compaction of initially loose "Skarpa" sand after reaching the instability line, cf. Fig. 6

5.2. Theoretical prediction

In order to predict the behaviour shown in Figs. 6 and 7, incremental equation $(4.1)_1$ in Part I will be modified. This modification is necessary as $dq = 0$ along the paths BCD, but η increases, which means deviatoric loading. In this special case, there is also $dp' < 0$, which means spherical unloading. The starting point to the modification is again Eq. (3.5) in Part I which can be re-written in the following form

$$\varepsilon_v = \sqrt{p'}c_1\eta^4 \tag{5.1}$$

The increment of the volumetric strain due to deviatoric loading is

$$d\varepsilon_v = \frac{\partial \varepsilon_v}{\partial p'}dp' + \frac{\partial \varepsilon_v}{\partial \eta}d\eta \tag{5.2}$$

Recall that $dq = 0$, therefore

$$d\eta = -\frac{q}{(p')^2}dp' \tag{5.3}$$

Equations (5.1)-(5.3) lead to the following formula

$$d\varepsilon_v = -3.5q^4c_1(p')^{-4.5}dp' \tag{5.4}$$

We have to add the component corresponding to spherical unloading to the RHS of this equation. Therefore, the volumetric strains that develop along

the paths BCD (see inset in Fig. 6) are given by the following incremental equation

$$d\varepsilon_v = \Big[\frac{A_v^u}{2\sqrt{p'}} - 3.5q^4c_1(p')^{-4.5}\Big]dp' \tag{5.5}$$

Integration of this equation, with the initial condition $\varepsilon_v(p' = p'_A) = 0$, leads to the following formula

$$\varepsilon_v = A_v^u(\sqrt{p'} - \sqrt{p'_A}) + c_1q^4[(p')^{-3.5} - (p'_A)^{-3.5}] \tag{5.6}$$

It should be remembered that volumetric strain (5.6) is imposed on the volumetric strains that have been developed along the path OAB, but for the sake of simplicity, the zero initial condition was assumed. Figure 8 illustrates Eq. (5.6) for the following data: $p'_A = 2$; $c_1 = 2.7$; $A_v^u = 4.4$. The qualitative agreement with the experimental data from Figs. 6 and 7 is achieved.
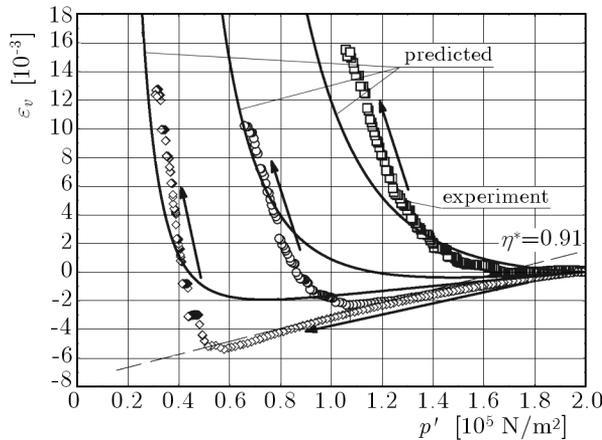

Fig. 8. The volumetric strains that develop during spherical unloading – theoretical prediction, cf. Figs. 6 and 7

6. Static liquefaction

Previous examples of prediction dealt with the fully drained conditions, when $u = 0$ and $\boldsymbol{\sigma} = \boldsymbol{\sigma'}$. The undrained conditions are described in Section 6 of Part I of this paper. It will be shown that the incremental model, proposed in the present paper, gives also good predictions for undrained conditions. It is known, from experimental investigations, that the undrained behaviour of

initially contractive and dilative soils differ. A characteristic feature of initially contractive soils is that they liquefy under shearing in undrained conditions, see e.g. Castro (1975); Konrad (1993); Lade (1992). The volumetric strains that for the initially contractive soil can be described by similar equations to those presented in Section 5.2, are zero during undrained shearing. These equations, combined with condition (6.1) in Part I, lead to the following expression

$$d\varepsilon_v = \frac{\partial \varepsilon_v^q}{\partial p'}dp' + \frac{\partial \varepsilon_v^q}{\partial \eta}d\eta + \frac{A_v^u}{2\sqrt{p'}}dp' = 0 \tag{6.1}$$

where ε_v^q is given by Eq. (5.1). Simple manipulations lead to the following differential equation describing the changes of the mean effective stress

$$\frac{dp'}{p'} = -\frac{6\eta^3}{\eta^4 + \frac{A_v^u}{c_1}}d\eta \tag{6.2}$$

Integration of this equation, with the initial condition $p' = p_0$ for $\eta = 0$, where p_0 is the initial confining stress, leads to the following formula

$$p' = p_0\sqrt{\left(\frac{1}{1 + \frac{c_1}{A_v^u}\eta^4}\right)^3} \tag{6.3}$$

The above equations allow for determination of the effective stress path during the undrained shearing. For example, Fig. 9 shows such a path for the data from Section 5.2. The predicted curve does not reproduce the experimental data too well from the quantitative point of view, although the qualitative agreement is good (solid line in Fig. 9). Small correction of the values of material parameters ($A_v^u = 0.8$; $c_1 = 2.4$) leads to the almost perfect agreement (dashed line in Fig. 9).

Figure 9 shows that the maximum shear stress supported by the saturated soil coincides with the instability line. After reaching this line, the deviatoric stress decreases, finally approaching the Coulomb-Mohr failure envelope. This phenomenon is designated as static liquefaction. The results presented in this Section show that the incremental model of the pre-failure behaviour of sand leads to realistic predictions in the case of undrained shearing of the initially contractive soil.

7. Undrained behaviour of dilative soil

The initially dilative sands behave in a different way than that shown in the previous Section. In order to make the analysis easy, let us simplify the beha-
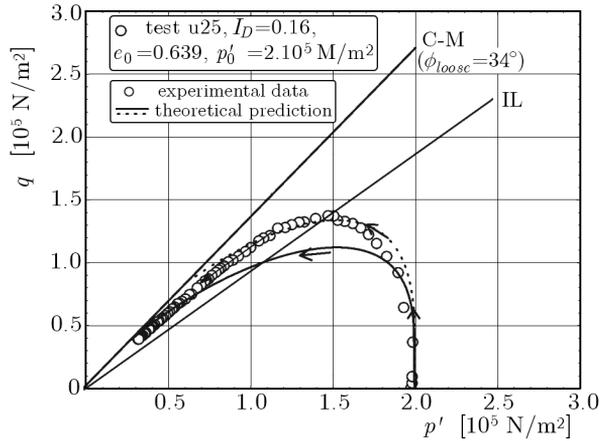
Fig. 9. Static liquefaction of initially contractive sand

viour shown in Fig. 6 inPart I, see Sawicki and Świdziński (2007). The bi-linear approximation is the following

$$
\varepsilon_v^q =
\begin{cases}
B_v \eta \sqrt{p'} & \text{for} \quad 0 \leqslant \eta \leqslant \eta' \\
\sqrt{p'}(C_v \eta + D_v) & \text{for} \quad \eta' \leqslant \eta \leqslant \eta''
\end{cases}
\tag{7.1}
$$

where B_v, C_v and D_v are certain coefficients. In the case considered: $B_v = 1.195$; $C_v = -77.8$; $D_v = 79.26$.

The already known procedure leads to the following formulae for the mean effective pressure

$$
p' =
\begin{cases}
p_0\left(1 + \dfrac{B_v}{A_v^u \eta}\right)^{-2} & \text{for} \quad 0 \leqslant \eta \leqslant \eta' \\
p * \left(\dfrac{\eta' + \xi}{\eta + \xi}\right)^2 & \text{for} \quad \eta' \leqslant \eta \leqslant \eta''
\end{cases}
\tag{7.2}
$$

where p^* corresponds to the mean effective stress on the instability line, and $\xi = (A_v + C_v)/D_v$. Figure 10 shows the effective stress paths for the above data and $A_v = 3.47$; $A_v^u = 2.91$, $\eta' = 1$; $\eta'' = 1.4$ for different initial confining stresses. The behaviour shown in Fig. 10 remains in a good agreement with the experimental results, which supports the thesis that our incremental model well describes the pre-failure behaviour of sands.

The characteristic feature of the behaviour shown in Fig. 10 is that, before reaching the instability line, the effective stress path is similar to that of the initially contractive soil, cf. Fig. 9. After reaching the instability line, the stress path turns right and both q and p' increase.
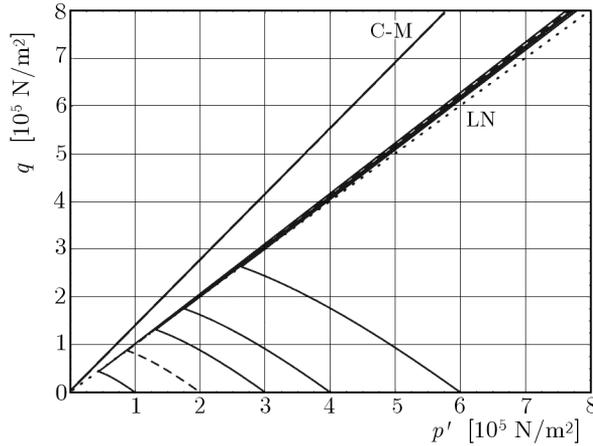
Fig. 10. Predicted effective stress paths during undrained shearing of sand

8.   Conclusions

In Part II of the present paper, it was shown that the incremental model describing the pre-failure behaviour of saturated sand leads to realistic predictions for various stress paths, different from those used for its calibration. The predictions of the model were determined for both the fully drained and undrained conditions. In all the cases analysed, the qualitative agreement between the predictions and experimental data is good. The qualitative agreement, for the average values of soil parameters, is also acceptable.

References

1. Castro G., 1975, Liquefaction and cyclic mobility of saturated sands, *J. Geotech. Engrg. ASCE*, **101**, GT6, 551-569

2. Konrad J.-M., 1993, Undrained response of loosely compacted sands during monotonic and cyclic compression tests, *Geotechnique*, **43**, 1, 69-89

3. Lade P.V., 1992, Static instability and liquefaction of loose fine sandy slopes, *J. Geotech. Engrg. ASCE*, **118**, 1, 51-70

4. Sawicki A., Świdziński W., 1998, Elastic moduli of particulate materials, *Powder Technology*, **96**, 24-32

5. Sawicki A., Świdziński W., 2007, Drained against undrained behavior of granular soils, *Arch. of Hydro-Engineering and Environ. Mech.*, **54**, 3, 207-222

6. Skopek P., Morgenstern N.R., Robertson P.K., Sego D.C., 1994, Collaps of dry sand, *Can. Geotech. J.*, **31**, 1008-1014

7. Świdziński W., 2006, *Compaction and Liquefaction Mechanisms of Non-Cohesive Soils*, IBW PAN, pp. 265 [in Polish]

Związki naprężenie-odkształcenie dla piasków suchych i nawodnionych Część II: Predykcje

Streszczenie

W części II przedstawiono predykcje modelu przyrostowego dla ścieżek naprężenia innych niż te stosowane przy kalibracji. Równania przyrostowe scałkowano dla ścieżek naprężenia i odkształcenia odpowiadających następującym warunkom: anizotropowa konsolidacja, warunki edometryczne, standardowa próba trójosiowa, sferyczne odciążenie przy stałym dewiatorze oraz ścinanie nawodnionego gruntu w warunkach bez odpływu wody z porów. Rozpatrzono reakcję gruntu w początkowym stanie dylatywnym i kontraktywnym. Predykcje teoretyczne porównano z wynikami doświadczeń. Wykazano dobrą zgodność tych predykcji z eksperymentem.